AerospaceEurope Conference2021
WARSAW, POLAND | 23 -26 NOVEMBER 2021
CEAS Council of European Aerospace Societies

A HYBRID VEM/BEM NUMERICAL TECHNIQUE FOR SIMULATING DAMAGE IN COMPOSITE MATERIALS

Lo Cascio M[1], Milazzo A[1] & Benedetti I[1]

[1]Department of Engineering, University of Palermo, Viale delle Scienze, Edificio 8, 90128, Palermo, Italy

Abstract

Composite materials are nowadays widely used in the aerospace sector both for primary and secondary structures for their high mechanical properties and the ability to model them according to project needs. Therefore, accurately predicting material behaviour when subjected to operating loads is extremely important in making the design process more efficient. For this purpose, computational approaches based on continuum damage mechanics have been largely used to study the progressive loss of material integrity due to the propagation and coalescence of microscopic defects.

In this contribution, a recently developed hybrid computational technique, which combines the Virtual Element Method (VEM) with the well-known Boundary Element Method (BEM), is employed to study unidirectional fibre-reinforced composite material's transverse behaviour in the presence of inclusions with complex geometries. BEM is used to model the stiffer inclusion phase, which is considered a linear elastic material and maintains its pristine state. VEM is adopted to study the softer matrix phase, using VEM's peculiar feature, which can simulate general nonlinear phenomena with a straightforward implementation like that of the standard FEM one. An application of the hybrid formulation mentioned above is presented to simulate damage onset and propagation in the matrix phase of the transverse section of a composite unite cell. Numerical results are discussed and compared with known results available in the relevant literature.

Keywords: Fibre-reinforced Composite Materials; Computational Micro-mechanics; Computational Homogenization; Virtual Element Method; Boundary Element Method

1. Introduction

The analysis and design of novel materials for different structural applications is frequently driven by the capacity to engineer their microstructure by proper coupling of different phases whose interaction is optimized to obtain desired properties at the scale of the considered application. Within this framework, computational micro-mechanics plays a significant role.

This contribution describes the application of a recently developed numerical technique [1, 2, 3] coupling the Virtual Element Method (VEM) with the Boundary Element Method (BEM) for the analysis of heterogeneous materials with damage.

VEM [4] extends the peculiarities of FEM to very general polygonal and polyhedral mesh elements, including irregular or non-convex elements as well as elements featuring curved boundaries. For such a reason, VEM provides a powerful, flexible tool for computational micro-mechanics problems, which frequently feature phases with complex geometries that may also show non-linear constitutive responses [5, 6, 7].

BEM [8, 9] is a numerical technique widely employed for the solution of several classes of problems in solids and materials mechanics, including computational homogenization of materials with complex morphology or constitutive behavior [10, 11, 12, 13, 14, 15, 16]. Based on a boundary integral reformulation of the considered problem, BEM enables decreasing the analysis dimensionality, e.g. from volumes to surfaces, resulting in substantial simplification of the pre-processing stage and in the reduction of the number of degrees of freedom, without penalties on the solution accuracy.

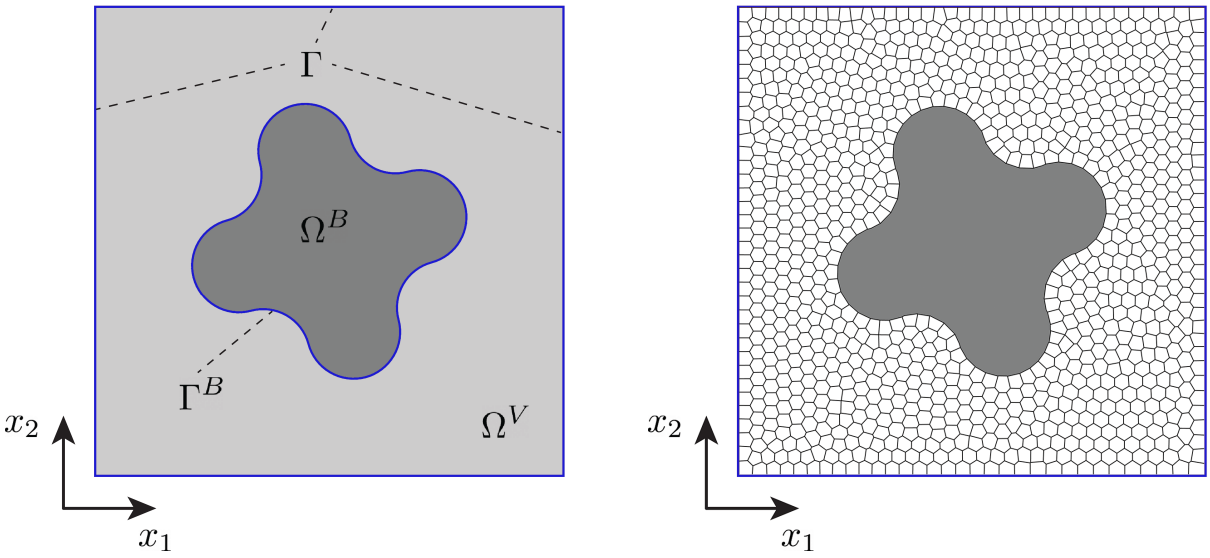

Figure 1 – A sample VEM/BEM analysis domain: geometry (left) and mesh (right).

This contribution is organized as follows: Section 2provides a brief overview of the employed formulation; Section 3reports an application to a fibre-reinforced composite material developing damage in the matrix phase.

2. Formulation

The multi-region two-dimensional domain $\Omega \subset \Re^2$ with external boundary Γ, shown in Fig. 1, is considered in this study. It is assumed that no body forces act within Ω, but either displacements or tractions can be enforced on the boundary Γ. The problem domain Ω is the union of two sub-domains, namely Ω^B and Ω^V, which represent, respectively, the transverse section of a fibre and the surrounding polymer matrix in a polymer fibre-reinforced composite. The two sub-domains share the interface $S \equiv \Gamma^B$. BEM is used to model the fibre inclusion, which is supposed to behave within the linear elastic range. VEM is used to model the surrounding matrix, developing more complex non-linear behaviours, offering the advantage of extended flexibility in terms of element topology and shapes. VEM ensures convergence and accuracy for highly distorted meshes and even non-convex elements, considered pathological and problematic in standard FEM analyses. Such a characteristic relieves the quality requirements for the employed meshes, thus reducing the need for mesh consistency checks in the pre-processing stage of the analysis, which may prove highly beneficial when a large number of morphologies have to be generated and analysed, as often the case in computational micromechanics [6].
For the analysis, Ω^V is partitioned into several polygons of general shape, while the boundary $S \equiv \Gamma^B$ is divided into several straight segments, which form the edges of the polygonal elements in Ω^V lying in the proximity of the interface between the two sub-domains, see Fig. 1. Further details on the adopted meshing procedures and related convergence analyses can be found in Ref. [3].

2.1 Boundary Element modeling of the inclusion

For the sub-domain Ω^B with smooth boundary $S = \Gamma^B$, if no body forces are applied, the boundary integral equation (BIE) for the displacements components u_j at a boundary *collocation* point $\mathbf{x}_0 \in S$ can be written, using tensor notation with $i, j = x, y$, as in Ref. [8].

$$\frac{1}{2} u_j(\mathbf{x}_0) = \int_S G_{ij}(\mathbf{x}_0, \mathbf{x})\, t_j(\mathbf{x})\, ds - \int_S H_{ij}(\mathbf{x}_0, \mathbf{x})\, u_j(\mathbf{x})\, ds \tag{1}$$

where $u_i(\mathbf{x})$ and $t_i(\mathbf{x})$ are the displacement and traction components at the *integration* boundary point $\mathbf{x}$, $G_{ij}(\mathbf{x}_0, \mathbf{x})$ and $H_{ij}(\mathbf{x}_0, \mathbf{x})$ are, respectively, the components of the two-dimensional elasto-static fundamental solution for displacements and tractions under plane strain assumptions. The numerical treatment of the boundary integral formulation expressed by Eq. (1) is based on the subdivision of

the boundary S into a collection of m straight elements ΔS_k and a convenient approximation of the boundary displacement and traction components in terms of shape functions and nodal values. A linear approximation of displacements and tractions over each boundary element

$$\mathbf{u}(\xi) = \mathbf{N}(\xi)\,\mathbf{u}^k, \qquad \mathbf{t}(\xi) = \mathbf{N}(\xi)\,\mathbf{t}^k \tag{2}$$

is assumed, where $\mathbf{N}(\xi) \in \mathbb{R}^{2\times 4}$ is the matrix collecting one.dimensional linear shape functions for the boundary segment ΔS_k, expressed as function of the natural coordinate ξ, and $\mathbf{u}^k, \mathbf{t}^k \in \mathbb{R}^{4\times 1}$ collect, respectively, nodal components of displacements and tractions associated with the boundary segment ΔS_k. This approach assures a straightforward treatment of the interface conditions between the boundary element and the VEM elements used to model the contiguous matrix.
Using the procedures described, e.g., in Ref. [9], Eq. (1) can be numerically integrated. Such numerical integration, repeated for Eq. (1) written for the set of all the collocation points chosen along the boundary S, leads to the global system of linear algebraic equations

$$\mathbf{H}\,\mathbf{U}^{\mathsf{B}} = \mathbf{G}\,\mathbf{T}^{\mathsf{B}} \tag{3}$$

where the vectors $\mathbf{U}^{\mathsf{B}}, \mathbf{T}^{\mathsf{B}} \in \mathbb{R}^{2m\times 1}$ collect the components of displacements and tractions of all collocation nodes identified along the boundary S and $\mathbf{H}, \mathbf{G} \in \mathbb{R}^{2m\times 2m}$ collect the coefficients obtained from the numerical integration of Eq. (1) associated to such collocation points. Since the BEM domain identifies an inclusion in the analyzed domain, both $\mathbf{U}^{\mathsf{B}}$ and $\mathbf{T}^{\mathsf{B}}$ are unknown quantities that must be determined from the analysis.

2.2 Virtual Element modeling of the matrix

A lowest-order VEM formulation is employed to model the domain Ω^{V}.
For a general polygonal element E, the element degrees of freedom are the values of the displacements components at each of its n vertex, which are collected into the vector $\mathbf{u}_E$. Analogously to the standard FEM, the displacements field $\mathbf{u}$ is expressed as

$$\mathbf{u} = \mathbf{N}(\xi,\eta)\,\mathbf{u}_E \tag{4}$$

where $\mathbf{N}(\xi,\eta)$ is the matrix containing the *virtual* shape functions $N_v(\xi,\eta)$ associated with each vertex v. Differently from standard FEM however, such shape functions are known only on the element edges of E, where they are globally continuous linear polynomials. Since the shape functions $N_v(\xi,\eta)$ are not explicitly known within the polygonal element, an explicit expression for the strains is not available. An approximated constant strain field ε_Π is assumed within each element, which can be computed from the degrees of freedom $\mathbf{u}_E$ as

$$\varepsilon_\Pi = \Pi_E\,\mathbf{u}_E \tag{5}$$

where $\Pi_E \in \mathbb{R}^{3\times 2n}$ is the matrix representation of a projection operator defined as [17]

$$\Pi_E = \frac{1}{A_E}\sum_{v=1}^{n}\int_{e_v} \mathbf{N}_v^E\,\mathbf{N}(\eta)\,ds, \qquad \mathbf{N}_v^E = \begin{bmatrix} n_x & 0 & n_y \\ 0 & n_y & n_x \end{bmatrix}^{\mathsf{T}} \tag{6}$$

where A_E is the area of the polygonal element E, bounded by its n edges e_v and $\mathbf{N}_v^E$ is the matrix containing the components n_x and n_y of the outward unit normal vector over each edge. Since the restriction of the virtual shape functions N_v to such edges are known piece-wise linear polynomials, the integrals appearing at the right-hand side of Eq. (6) are exactly computable.
The VEM stiffness matrix $\mathbf{K}_E$ for a general polygonal element E is given by the sum of two terms

$$\mathbf{K}_E = \mathbf{K}_E^c + \mathbf{K}_E^s \tag{7}$$

The *consistency* contribution is given by

$$\mathbf{K}_E^c = A_E\,\Pi_E^{\mathsf{T}}\,\mathbf{C}^0\,\Pi_E \tag{8}$$

where $\mathbf{C}^0$ is the material stiffness tensor in Voigt notation. $\mathbf{K}_E^s$ is a *stabilization* term whose presence is motivated by the need to avoid zero-energy modes not associated with rigid body motion, which may arise as a consequence of the fact that the approximate strains ε_Π are assumed constant within the element, while the displacements $\mathbf{u}$ are piece-wise linear on the element edges, which in general may induce incompatibility between ε_Π and the nodal degrees of freedom $\mathbf{u}_E$. Details of the computation of such term can be found in Ref. [4].
The equivalent nodal forces $\mathbf{F}_E$ are computed as in the standard FEM from specified tractions $\bar{\mathbf{t}}$ over the element boundary $\partial E = \bigcup e_v$, i.e.

$$\mathbf{F}_E = \int_{\partial E} \mathbf{N}^{\mathsf{T}}(\xi,\eta)\,\bar{\mathbf{t}}\,ds \tag{9}$$

Once the elemental stiffness matrices and load vectors are built, the assembly of the VEM global matrices and vectors can be performed following the standard FE procedures, to obtain the following sets of equations for the VEM sub-domain

$$\mathbf{K}^{\mathsf{V}}\mathbf{U}^{\mathsf{V}} = \mathbf{F}^{\mathsf{V}} \tag{10}$$

where $\mathbf{K}^{\mathsf{V}}$, $\mathbf{U}^{\mathsf{V}}$ and $\mathbf{F}^{\mathsf{V}}$ are, respectively, the stiffness matrix, the nodal displacement vector and the force vector, with the superscript V introduced to identify quantities related with the VEM domain.

2.2.1 Modeling damage with Virtual Elements

The Virtual Element formulation can be extended to problems involving nonlinear material behaviors [18, 19]. An *isotropic damage model* [20, 21, 22, 23] is chosen to model the matrix phase of the composite material. Consequently, the loss of material integrity is caused by an equal degradation of the bulk and shear moduli, and it is governed by a single internal scalar *damage variable* ω, which tracks and measures the loss of stiffness of the material. Damage evolves monotonically within its admissible range $0 \leq \omega \leq 1$, where 0 is associated with the pristine state and 1 with the fully degraded material. The constitutive equations for an isotropic damage model are defined as

$$\boldsymbol{\sigma} = (1-\omega)\,\mathbf{C}^0\,\varepsilon_\Pi \tag{11}$$

where σ and ε_Π collect the Voigt components of the stress and strain respectively, and $\mathbf{C}^0$ is the elasticity matrix for the pristine elastic material. Damage evolution is triggered upon fulfillment of the condition

$$F(\varepsilon) = \tau(\varepsilon) - r = 0, \qquad r = \max_{\lambda\in\mathscr{H}}\{\tau(\lambda)\} \tag{12}$$

where $\tau(\varepsilon)$ is a suitably chosen norm of the strains, used to determine if the considered stress state belongs to the elastic domain, when $F(\varepsilon) < 0$, or if it induces damage initiation or evolution, $F(\varepsilon) = 0$. The monotonically increasing internal variable r represents the damage threshold at the current loading step λ and it is a function of the loading history $\mathscr{H}$. To model the onset and evolution of damage in epoxy resins, often used as the matrix material in fibre-reinforced composites, Melro et al. [24] proposed an expression which reads

$$\tau(\varepsilon) = \frac{3\tilde{J}_2}{X_m^c X_m^t} + \frac{\tilde{I}_1(X_m^c - X_m^t)}{X_m^c X_m^t}, \tag{13}$$

where X_m^t and X_m^c are, respectively, the tensile and compressive strengths of the epoxy resin. $\tilde{I}_1$ and $\tilde{J}_2$ are, respectively, the first stress invariant and the second deviatoric stress invariant, both defined using the components of the effective stress $\tilde{\sigma} = \mathbf{C}^0\,\varepsilon_\Pi$ acting in the undamaged material. The evolution of damage is governed by the Kuhn-Tucker flow rules, which read

$$F \leq 0, \quad \dot{r} \geq 0, \quad \dot{r}F = 0, \tag{14}$$

and allow to distinguish between loading and unloading conditions. Unloading occurs when $\dot{\tau} \leq 0$; otherwise, damage evolves and the following consistency condition must be satisfied

$$\dot{F} = \dot{\tau} - \dot{r} = 0. \tag{15}$$

The exponential softening damage evolution law defined as in Ref. [25] as

$$\omega(r) = \left[1 - \frac{r_0}{r}\exp\left(-\frac{r-r_0}{r_f-r_0}\right)\right]\cdot H(r-r_0), \qquad r = \max_{\lambda\in\mathscr{H}}\{\tau(\lambda)\} \tag{16}$$

is adopted to model the evolution of the damage ω after its onset. $H(\cdot)$ denotes the Heaviside step function, the parameter r_0 identifies the damage initiation condition and r_f specifies the softening response behavior.
The nonlinear constitutive laws appearing in Eq. (11) can be treated, as in nonlinear finite element formulations, using standard incremental-iterative algorithms. The stress at a generic point $\mathbf{x}$ and at a generic loading step λ is given by the expression

$$\sigma = \sigma(\lambda, \mathbf{x}, \varepsilon_\Pi, \mathscr{H}), \tag{17}$$

where ε_Π is the approximated virtual strain computed as in Eq. (5), using the matrix projector operator Π and $\mathscr{H}$ contains the history variables of the damage model. The tangent material stiffness matrix $\mathbf{C}_{tan}$ at a certain time t is consistently computed from the constitutive law in Eq. (17) as

$$\mathbf{C}_{tan}(t, \mathbf{x}, \varepsilon_\Pi, \mathscr{H}) = \frac{\partial\sigma}{\partial\varepsilon_\Pi}. \tag{18}$$

2.3 Procedure to couple BEM and VEM subdomains

Coupling between BEM and VEM subdomains is achieved according to the approach described in Ref. [3]. The BEM subdomain is treated as a macro-finite element, and the *traction*-displacement equations associated with it are transformed into *force*-displacement equations and assembled with the VEM equations, already expressed in terms of nodal forces and displacements.
The vectors $\mathbf{U}^{\mathsf{V}}$ and $\mathbf{F}^{\mathsf{V}}$ appearing in Eq. (10) collect the displacement and nodal force components of all the nodes in the VEM domain. It is possible to partition the vectors as

$$\mathbf{U}^{\mathsf{V}} = \begin{bmatrix} \mathbf{U}^{\mathsf{V}}_S \\ \mathbf{U}^{\mathsf{V}}_D \end{bmatrix}, \qquad \mathbf{F}^{\mathsf{V}} = \begin{bmatrix} \mathbf{F}^{\mathsf{V}}_S \\ \mathbf{F}^{\mathsf{V}}_D \end{bmatrix}, \tag{19}$$

where $\mathbf{U}^{\mathsf{V}}_S$ and $\mathbf{F}^{\mathsf{V}}_S$ identify components related to nodes belonging to the interface S. Along S, the nodal displacements and forces must satisfy the compatibility and equilibrium conditions

$$\mathbf{U}^{\mathsf{B}} = \mathbf{U}^{\mathsf{V}}_S, \qquad \mathbf{F}^{\mathsf{B}} + \mathbf{F}^{\mathsf{V}}_S = \mathbf{0}, \tag{20}$$

which have been written considering that no external nodal forces act on the nodes belonging to S. The displacement compatibility equations can be readily written, as the same displacement components appear in both the BEM and VEM equations. Contrarily, while nodal forces appear in Eq. (10), related to the VEM domain, tractions appear in Eq. (3), related to the BEM domain, so that it is necessary to retrieve consistent nodal forces from BEM tractions before writing the equilibrium equations appearing in Eq. (20). This may be done by resorting to appropriate energetic considerations, which allow associating a system of equivalent nodal forces $\mathbf{F}^{\mathsf{B}}$ with the tractions acting over the considered boundary elements leading to

$$\mathbf{F}^{\mathsf{B}} = \mathbf{M}\mathbf{T}^{\mathsf{B}}, \tag{21}$$

where $\mathbf{F}^{\mathsf{B}}, \mathbf{T}^{\mathsf{B}} \in \mathbb{R}^{2m\times 1}$ and $\mathbf{M} \in \mathbb{R}^{2m\times 2m}$, being m the total number of boundary nodes/elements, see Refs.1-2 for details. From Eq. (3), it follows $\mathbf{T}^{\mathsf{B}} = \mathbf{G}^{-1}\mathbf{H}\mathbf{U}^{\mathsf{B}}$, so that Eq. (21) can be rewritten as the following force-displacement equilibrium equation

$$\mathbf{F}^{\mathsf{B}} = \mathbf{M}\mathbf{T}^{\mathsf{B}} = \left(\mathbf{M}\mathbf{G}^{-1}\mathbf{H}\right)\mathbf{U}^{\mathsf{B}} = \mathbf{K}^{\mathsf{B}}\mathbf{U}^{\mathsf{B}}. \tag{22}$$

Eq. (10), related to the VEM sub-domain, can be conveniently rewritten as

$$\begin{bmatrix} \mathbf{K}^{\mathsf{V}}_{SS} & \mathbf{K}^{\mathsf{V}}_{SD} \\ \mathbf{K}^{\mathsf{V}}_{DS} & \mathbf{K}^{\mathsf{V}}_{DD} \end{bmatrix} \begin{bmatrix} \mathbf{U}^{\mathsf{V}}_S \\ \mathbf{U}^{\mathsf{V}}_D \end{bmatrix} = \begin{bmatrix} \mathbf{F}^{\mathsf{V}}_S \\ \mathbf{F}^{\mathsf{V}}_D \end{bmatrix}, \tag{23}$$

and it may be eventually combined with the interface conditions in Eq. (20), with Eq. (22) and with suitable external boundary conditions to obtain the problem solution.

3. Numerical experiment

An application of the hybrid virtual-boundary element formulation, combined with an isotropic damage model for the regions modelled with virtual elements, is reported in this Section.

Fig. 2 shows the model's geometry and boundary conditions: a unit cell comprising a single fibre embedded in an epoxy matrix, with initial partial debonding between fibre and matrix along the region of the interface identified by $|\theta_d| \leq 70^\circ$. Outside the debonded region, the inclusion is perfectly bonded to the matrix. The study of this fibre-matrix system has been treated extensively [26, 27, 28].

The present test aims at simulating the progression into the matrix of the two kinked cracks that start from both ends of the debonded zone. It is worth noting that, in this specific application, the coupling procedure detailed in Section 2.3 is applied only over the pristine region of the matrix-fibre interface. The debonded regions require zero traction conditions over the edges of the BEM fibre domain and zero nodal equivalent forces over the nodes at the edge of the VEM matrix domain.

The side length of the unit cell is $L = 0.2\,\text{mm}$ and the fibre diameter is $D = 0.025\,\text{mm}$. The centre of the circle coincides with the centre of the square. The tensile loading is applied by prescribing uniform displacements $\bar{u}$ at the sample left and right edges. Plane strain conditions are assumed. The fibre material is assumed linear elastic, and it does not develop damage. The matrix material is treated as linear elastic until the damage onset, governed by the loading function in Eq. (13). The exponential damage evolution law in Eq. (16) is assumed, with $r_0 = 1$, $r_f = 234$, according to strength and fracture toughness data about epoxy. The transverse elastic material parameters are $E_F = 201\,\text{GPa}$ and $\nu_F = 0.22$ for the fibre and $E_M = 2.8\,\text{GPa}$ and $\nu_M = 0.33$ for the matrix. The fracture toughness of the epoxy matrix is $G_{fr} = 0.09\,\text{N/mm}$.

A integral-type non local regularization approach [29, 30] is employed, which consists in replacing the local value of the equivalent strain $\tau(\mathbf{x}_p)$ at a certain point $\mathbf{x}_p$ with its weighted average $\bar{\tau}(\mathbf{x}_p)$ over a representative circular domain surrounding each material point $\mathbf{x}_p$

$$\bar{\tau}(\mathbf{x}_p) = \int_\Omega \alpha(\mathbf{x}_p, \mathbf{x}_q)\,\tau(\mathbf{x}_q)\,d\Omega, \tag{24}$$

where Ω is the analysis domain and $\alpha(\mathbf{x}_p, \mathbf{x}_q)$ is a nonlocal weight function chosen as

$$\alpha(\mathbf{x}_p, \mathbf{x}_q) = \frac{\alpha_0(r)}{\int_\Omega \alpha_0(r)\,d\Omega}, \tag{25}$$

where $\alpha_0(r)$ is a non-negative function of the distance $r = ||\mathbf{x}_p - \mathbf{x}_q||$ between two considered material points, monotonically decreasing for $r \geq 0$. The expression adopted for $\alpha_0(r)$ is the truncated quadratic polynomial function

$$\alpha_0(r) = \left\langle 1 - \frac{r^2}{R^2} \right\rangle^2, \tag{26}$$

where R is known as the *interaction radius* and it is a parameter related to the characteristic length l_c. In this test, a value of $R = D/3$ has been used.

8047 lowest-order virtual polygon elements are used to mesh the matrix region, and consequently, 256 one-dimensional linear boundary elements on the fibre-matrix interface. The simulation is performed under displacement control using a Newton-Raphson with adaptive load step to track the steep softening branch. The simulation is arrested at a nominal macro-strain $\varepsilon_x = 0.05$.

Fig. 3 shows the load-displacement diagram: for each load increment, the plotted reaction force is computed as the sum of the nodal reaction forces on the right edge. The identified labels correspond to the damage profiles shown in Fig. 4. Linear elastic behaviour is exhibited up to slightly before point (a) in the curve, which marks damage initiation at the ends of the debonded interface, where stress concentration is expected. Once the damage is activated, the two symmetric damaged/failed regions progress within the matrix, following a kinked path consistent with the previously cited references' behaviour. As the load increases, the material failure evolves, affecting regions oriented perpendicularly to the load direction up to the domain boundary, which causes a progressive decrease of the load-carrying capability identified by the softening branch of the load-displacement diagram.

4. Contact Author Email Address

Please contact the corresponding author at: marco.locascio01@unipa.it

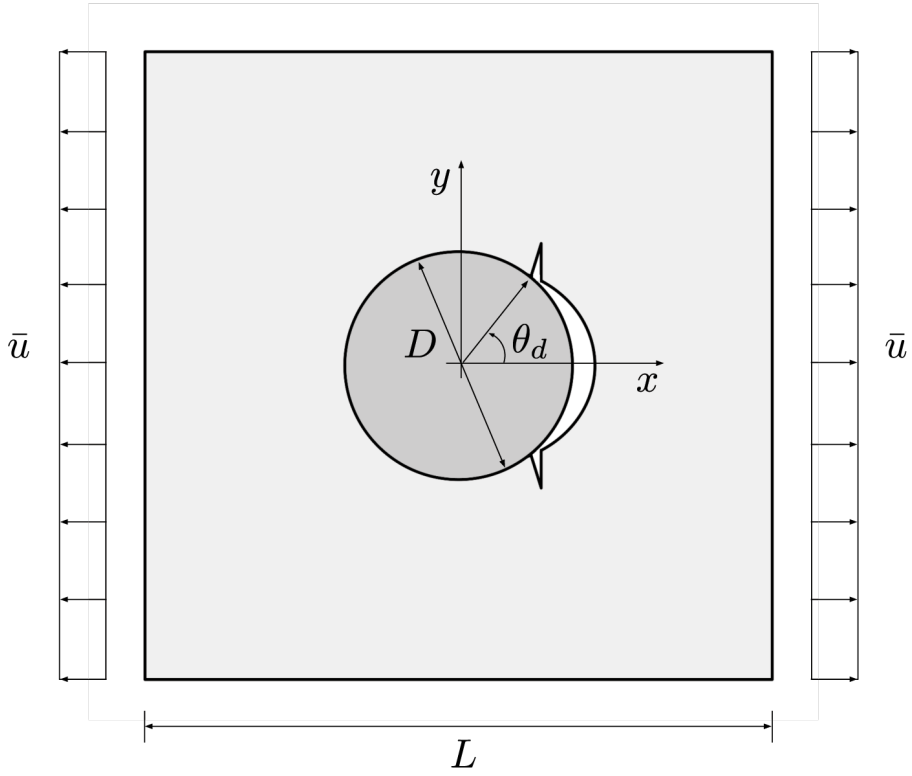

Figure 2 – Geometry and boundary conditions of the composite unit cell containing a circular fibre partially debonded from the matrix.

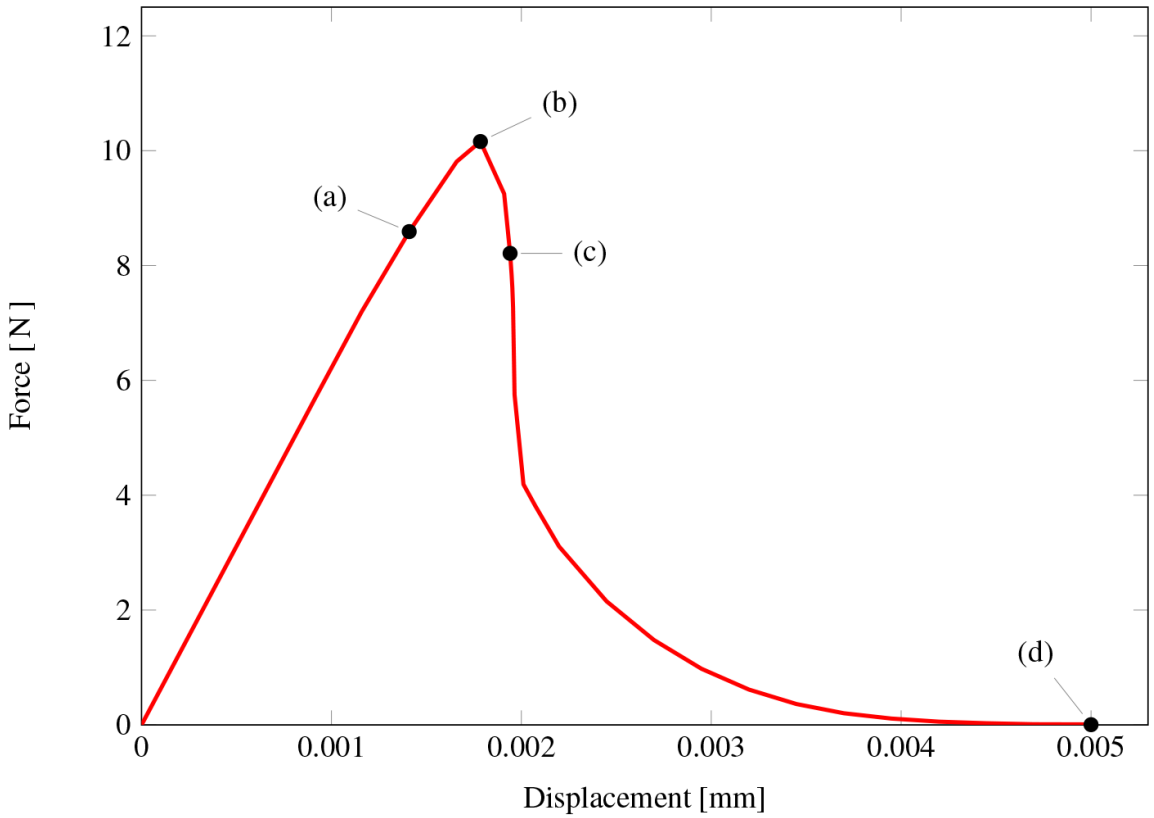

Figure 3 – Force-displacement diagram for the composite unit cell test.

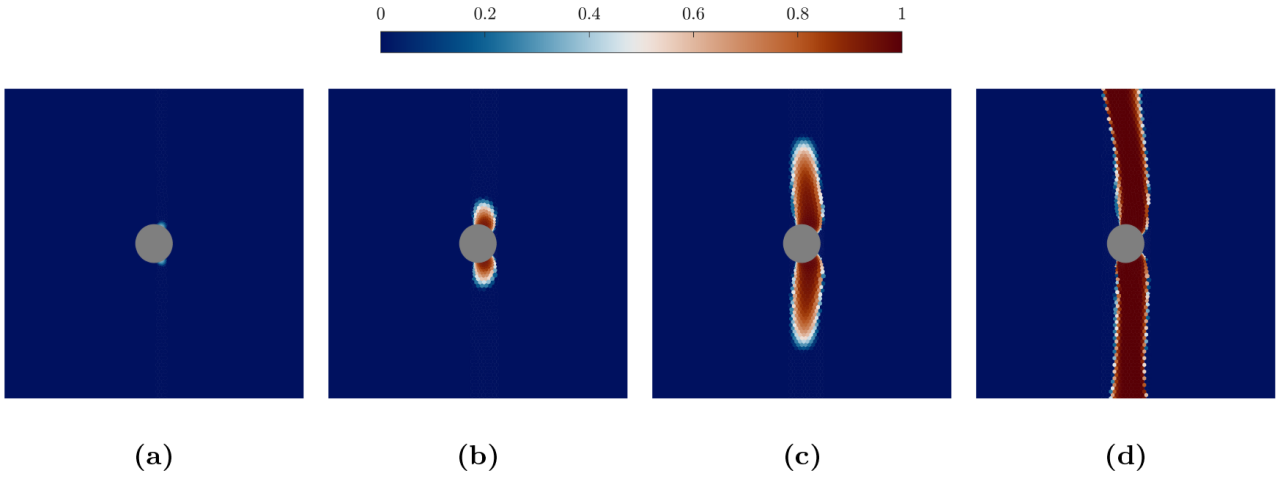

Figure 4 – Evolution of the damage profile for the composite unit cell test.

5. Copyright Statement

The authors confirm that they, and/or their company or organization, hold copyright on all of the original material included in this paper. The authors also confirm that they have obtained permission, from the copyright holder of any third party material included in this paper, to publish it as part of their paper. The authors confirm that they give permission, or have obtained permission from the copyright holder of this paper, for the publication and distribution of this paper as part of the AEC proceedings or as individual off-prints from the proceedings.

References

[1] Lo Cascio M, Grifo M, Milazzo A, Benedetti I. Computational Homogenization of Heterogeneous Materials by a Novel Hybrid Numerical Scheme. *Journal of Multiscale Modelling*, Vol. 11, No. 04, pp 66-88, 2020.

[2] Lo Cascio M, Benedetti I, Mantič V. Micro damage and cracking in fibre reinforced composites by a novel hybrid numerical technique. *AIP Conference Proceedings* Vol. 2309, 020001, 2020.

[3] Lo Cascio M, Milazzo A, Benedetti I. A hybrid virtual–boundary element formulation for heterogeneous materials. *International Journal of Mechanical Sciences*, Vol. 199, 106404, 2021.

[4] Beirão da Veiga L, Brezzi F, Cangiani A, Manzini G, Marini LD, Russo A. Basic principles of virtual element methods. *Mathematical Models and Methods in Applied Sciences*, Vol. 23, No. 1, pp 199-214, 2013.

[5] Artioli E, Marfia S, Sacco E. High-order virtual element method for the homogenization of long fiber nonlinear composites. *Computer Methods in Applied Mechanics and Engineering*, Vol. 341, pp 571-585, 2018.

[6] Lo Cascio M, Milazzo A, Benedetti I. Virtual element method for computational homogenization of composite and heterogeneous materials. *Composite Structures*, Vol. 232, 111523, 2020.

[7] Lo Cascio M, Milazzo A, Benedetti I. Virtual element method: Micro-mechanics applications. In: *Key Engineering Materials*, Vol. 827, pp 128-133 (Trans Tech Publications Ltd), 2020.

[8] Banerjee PK, Butterfield R. *Boundary element methods in engineering science*. McGraw-Hill London, 1981.

[9] Aliabadi MH, *The boundary element method, Volume 2: applications in solids and structures*. John Wiley & Sons, 2002.

[10] Benedetti I, Aliabadi MH. A three-dimensional cohesive-frictional grain-boundary micromechanical model for intergranular degradation and failure in polycrystalline materials. *Computer Methods in Applied Mechanics and Engineering*, Vol. 265, pp 36-62, 2013.

[11] Gulizzi V, Milazzo A, Benedetti I. An enhanced grain-boundary framework for computational homogenization and micro-cracking simulations of polycrystalline materials, *Computational Mechanics*, Vol. 56, pp 631-651, 2015.

[12] Benedetti I, Aliabadi MH. Multiscale modeling of polycrystalline materials: A boundary element approach to material degradation and fracture. *Computer Methods in Applied Mechanics and Engineering*, Vol. 289, pp 429-453, 2015.

[13] Benedetti I, Gulizzi V, Mallardo V. A grain boundary formulation for crystal plasticity. *International Journal of Plasticity*, Vol. 83, pp 202-224, 2016.

[14] Benedetti I, Gulizzi V. A grain-scale model for high-cycle fatigue degradation in polycrystalline materials. *International Journal of Fatigue*, Vol. 116, pp 90-105, 2018.

[15] Benedetti I, Gulizzi V, Milazzo A. A microstructural model for homogenisation and cracking of piezoelectric polycrystals. *Computer Methods in Applied Mechanics and Engineering*, Vol. 357, 112595, 2019.

[16] Parrinello F, Gulizzi V, Benedetti I. A computational framework for low-cycle fatigue in polycrystalline materials, *Computer Methods in Applied Mechanics and Engineering*, Vol. 383, 113898, 2021.

[17] Artioli E, Beirão da Veiga L, Lovadina C, Sacco E. Arbitrary order 2D virtual elements for polygonal meshes: part I, elastic problem. *Computational Mechanics*, Vol. 60, pp 355-377, 2017.

[18] Beirão da Veiga L, Lovadina C, Mora D. A virtual element method for elastic and inelastic problems on polytope meshes. *Computer Methods in Applied Mechanics and Engineering*, Vol. 295, pp 327-346, 2015.

[19] Artioli E, Beirão da Veiga L, Lovadina C, Sacco E. Arbitrary order 2d virtual elements for polygonal meshes: Part ii, inelastic problem. *Computational Mechanics*, Vol. 60, pp 643-657, 2017.

[20] Lemaitre J. Local approach of fracture. *Engineering Fracture Mechanics*, Vol. 25, pp 523-537, 1986.

[21] Simo JC, Ju J. Strain-and stress-based continuum damage models — i. formulation. *International Journal of Solids and Structures*, Vol. 23, pp 821-840, 1987.

[22] Simo JC, Ju J. Strain-and stress-based continuum damage models—ii. computational aspects, *International Journal of Solids and Structures*, Vol. 23, pp 841-869, 1987.

[23] Chaboche JL. Continuum Damage Mechanics: Part I – General Concepts. *Journal of Applied Mechanics*, Vol. 55, pp 59-64, 1988.

[24] Melro A, Camanho P, Pires FA, Pinho S. Micromechanical analysis of polymer composites reinforced by unidirectional fibres: Part i–constitutive modelling. *International Journal of Solids and Structures*, Vol. 50, pp 1897-1905, 2013.

[25] Jirásek M. Nonlocal damage mechanics. *Revue européenne de génie civil*, Vol. 11, pp 993-1021, 2007.

[26] París P, Correa E, Mantič V, Kinking of transversal interface cracks between fiber and matrix. *Journal of Applied Mechanics*, Vol. 74, pp 703-716, 2007.

[27] Mantič V. Interface crack onset at a circular cylindrical inclusion under a remote transverse tension. Application of a coupled stress and energy criterion. *International Journal of Solids and Structures*, Vol. 46, pp 1287-1304, 2009.

[28] Távara L, Mantič V, Graciani E, París F. Bem analysis of crack onset and propagation along fiber–matrix interface under transverse tension using a linear elastic–brittle interface model. *Engineering Analysis with Boundary Elements*, Vol. 35, pp 207-222, 2011.

[29] Pijaudier-Cabot G, Bažant ZP. Nonlocal damage theory. *Journal of Engineering Mechanics*, Vol. 113, pp 1512-1533, 1987.

[30] Jirásek M. Nonlocal models for damage and fracture: comparison of approaches. *International Journal of Solids and Structures*, Vol. 35, No. 31-32, pp 4133–4145, 1998.